JACS
JOURNAL OF THE AMERICAN CHEMICAL SOCIETY

Article

pubs.acs.org/JACS

Steric and Dynamic Parameters Influencing In Situ Cycloadditions to Form Triazole Inhibitors with Crystalline Acetylcholinesterase

Yves Bourne,*[,†,‡] K. Barry Sharpless,[§] Palmer Taylor,[∥] and Pascale Marchot*[,†,‡]

[†]Aix-Marseille Université, laboratory Architecture et Fonction des Macromolécules Biologiques, Faculté des Sciences de Luminy, 13288 Marseille cedex 09, France

[‡]Centre National de la Recherche Scientifique, laboratory Architecture et Fonction des Macromolécules Biologiques, Faculté des Sciences de Luminy, 13288 Marseille cedex 09, France

[§]Department of Chemistry, The Skaggs Institute for Chemical Biology, The Scripps Research Institute, La Jolla, California 92037, United States

[∥]Department of Pharmacology, Skaggs School of Pharmacy and Pharmaceutical Sciences, University of California at San Diego, La Jolla, California 92093-0650, United States

ABSTRACT: Ligand binding sites on acetylcholinesterase (AChE) comprise an active center, at the base of a deep and narrow gorge lined by aromatic residues, and a peripheral site at the gorge entry. These features launched AChE as a reaction vessel for in situ click-chemistry synthesis of high-affinity TZ2PA6 and TZ2PA5 inhibitors, forming a *syn*-triazole upon cycloaddition within the gorge from alkyne and azide reactants bound at the two sites, respectively. Subsequent crystallographic analyses of AChE complexes with the TZ2PA6 regioisomers demonstrated that *syn* product association is accompanied by side chain reorganization within the gorge, freezing-in-frame a conformation distinct from an unbound state or *anti* complex. To correlate inhibitor dimensions with reactivity and explore whether in situ cycloaddition could be accelerated in a concentrated, crystalline template, we developed crystal-soaking procedures and solved structures of AChE complexes with the TZ2PA5 regioisomers and their TZ2/PA5 precursors (2.1−2.7 Å resolution). The structures reveal motions of residue His447 in the active site and, unprecedentedly, residue Tyr341 at the gorge mouth, associated with TZ2 binding and coordinated with other side chain motions in the gorge that may guide AChE toward a transient state favoring *syn*-triazole formation. Despite precursor binding to crystalline AChE, coupling of rapid electric field fluctuations in the gorge with proper alignments of the azide and alkyne reactants to form the triazole remains a likely limiting step. These observations point to a prime requirement for AChE to interconvert dynamically between sequential conformations to promote favorable electrostatic factors enabling a productive apposition of the reactants for reactivity.

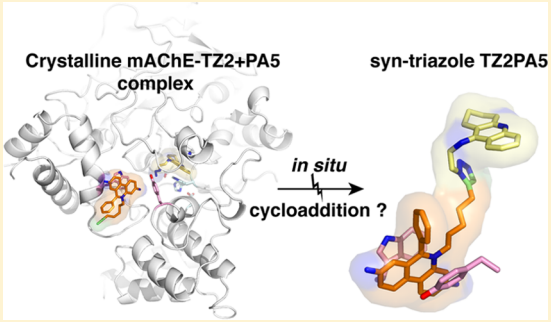

INTRODUCTION

The enzyme acetylcholinesterase (AChE) rapidly terminates cholinergic neurotransmission by catalyzing hydrolysis of the neurotransmitter, acetylcholine, at peripheral and central synapses. Inhibitors of AChE have been used for over a century in various therapeutic considerations.[1,2] Competitive reversible or irreversible inhibitors of AChE bind to the active center, which is located centrosymmetric to the ∼65 kDa subunit at the base of a ∼20 Å deep and narrow gorge, wherein lies the Glu/His/Ser catalytic triad.[3,4] A large permanent dipole moment of ∼1500 D roughly oriented along the axis of the active-site gorge characterizes the electrostatic field of AChE molecules and contributes to catalysis.[5,6] Noncompetitive, reversible inhibitors and activators bind the "peripheral anionic site" (PAS), an allosteric surface site located at the gorge entrance and encompassing overlapping subsites.[7,8] Other inhibitors harboring two functional binding moieties have the capability to bind both sites and line the gorge pathway. These bivalent inhibitors, which usually display greater affinities than individual components targeting a single site, simultaneously inhibit AChE catalysis and impair PAS functionality.[9]

The Huisgen 1,3-dipolar cycloaddition reaction between terminal azides and alkynes has become a powerful approach for drug discovery.[10−14] When these reactants are attached to a tricyclic tetrahydroacridine moiety as found in tacrine and a phenyl-phenanthridinium moiety as found in propidium (the "T-P library"), respectively selective for the active center and the PAS of AChE, the reaction is driven efficiently in situ, i.e., inside the active center gorge, and the gorge template preferentially catalyzes formation of a *syn*-triazole regioisomer inhibitor.[15−17] Inhibition measurements revealed a subpicomolar dissociation constant (K_i) for the *syn* TZ2PA6 regioisomer (3,8-diamino-6-phenyl-5-[6-[1-[2-[(1,2,3,4-tetrahydro-9-acridinyl)amino]ethyl]-1*H*-1,2,3-triazol-5-yl]hexyl]-phenanthridinium ($C_{42}H_{45}N_8$)) with association rate constants near the

Received: November 6, 2015
Published: January 5, 2016

DOI: 10.1021/jacs.5b11384
J. Am. Chem. Soc. 2016, 138, 1611−1621

diffusion limit for various AChE species including the original *Electrophorus electricus* AChE (EeAChE) and mouse AChE (mAChE) reaction vessels. The corresponding *anti* TZ2PA6 regioisomer (3,8-diamino-6-phenyl-5-[6-[1-[2-[(1,2,3,4-tetrahydro-9-acridinyl)amino]ethyl]-1*H*-1,2,3-triazol-4-yl]hexyl]-phenanthridinium ($C_{42}H_{45}N_8$)), not formed by the AChE molecule but generated in vitro, proved to be a respectable though weaker inhibitor with "only" near-picomolar K_i value for mAChE. Crystal structures of the *syn*- and *anti*-TZ2PA6-mAChE complexes pointed to substantial binding contribution from the triazole moiety within the gorge, along with large and unique conformational reorientation of Trp286 at the PAS associated with binding of the *syn* isomer, but not the *anti* isomer.[18] These structures also suggested that shortening the hexamethylene-azide linker by one carbon−carbon bond would favor intercalation of the PA moiety at the PAS and hence, the making of the higher affinity *syn* isomer. Compared with wild-type mAChE, a Tyr337Ala mutant affording an aromatic ring deletion in a constricted region of the gorge was found to display full catalytic activity, along with 2−3 orders of magnitude higher affinities for the *syn* and *anti* TZ2PA6 regioisomers, reflected in diffusion-limited association, dissociation half-times of ca. one month and 1 week, respectively, and femtomolar K_i values.[19] Structures of the cocrystallized complexes of the Tyr337Ala mutant with the two TZ2PA6 isomers revealed a slow, conformational remodeling of the bound regioisomers and their interacting side chains within the mAChE gorge, that correlates with the much slower dissociation rates of the solution complexes formed with the mutant, when compared with wild-type mAChE.[19]

A search for additional triazoles formed in situ from binary azide/alkyne mixtures, by extending the T-P library of building blocks and optimizing the LC/MS analytical method, led to the discovery of three new inhibitors from in situ reactions within EeAChE and mAChE templates.[16] These novel compounds, *syn*-TZ2PA5, *syn*-TA2PZ5 and *syn*-TA2PZ6, also derived from tacrine and phenyl phenanthridinium azides and alkynes, again proved to be extremely potent AChE inhibitors with dissociation constants in the picomolar range, consistent with those previously obtained for the TZ2/PA6 series.[15]

To document the structural bases for the differences in dissociation constants of the TZ2PA5 *anti* (3,8-diamino-6-phenyl-5-[6-[1-[2-[(1,2,3,4-tetrahydro-9-acridinyl)amino]-ethyl]-1*H*-1,2,3-triazol-4-yl]pentyl]-phenanthridinium ($C_{41}H_{45}N_8$)) versus *syn* (3,8-diamino-6-phenyl-5-[6-[1-[2-[(1,2,3,4-tetrahydro-9-acridinyl)amino]ethyl]-1*H*-1,2,3-triazol-5-yl]pentyl]-phenanthridinium ($C_{41}H_{45}N_8$)) regioisomers and of the TZ2PA5 versus TZ2PA6 inhibitors toward wild-type mAChE (Scheme 1, Table 1), we solved crystal structures of mAChE complexes with the *anti*- and *syn*-TZ2PA5 regioisomers and analyzed them comparatively with the TZ2PA6-mAChE structures.[18] Compared to the TZ2PA6 isomers, the bound TZ2PA5 molecules span the ∼20 Å mAChE gorge path in nearly identical fashion by anchoring to both the active center at the base of the gorge and the PAS at the gorge entrance. Yet, the *syn* TZ2PA5 complex is characterized by a novel and distinctive orientation of the phenyl-phenanthridinium moiety at the PAS, associated with an unprecedented conformational adaptation of mAChE residue Tyr341 at the rim of the gorge. Moreover, to explore whether the cycloaddition reaction would occur in crystallo, i.e., within a highly concentrated, tightly packed, nondiffusible AChE vessel, we set up crystal soaking procedures expected to favor the

Scheme 1. Structures of the PA5 and TZ2 Precursors and the *syn* and *anti* TZ2PA5 Regioisomers Formed by 1,3-Dipolar Cycloaddition[16,a]

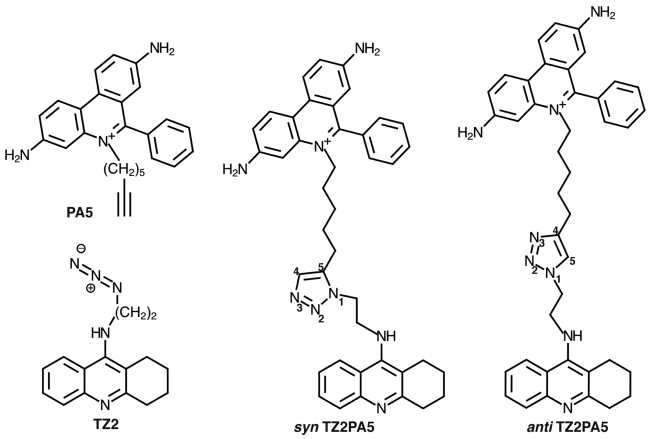

[a]The phenyl-phenanthridinium, $4_{anti}/5_{syn}$-triazole and tacrine moieties are shown from top to bottom.

trapping of properly oriented precursors and efficient cycloaddition of their reactant groups within the crystalline mAChE gorge. We then examined the subsequent crystallographic data sets to detect the presence of the triazole product. No triazole inhibitors could be observed, suggesting that they did not form in the crystalline mAChE template at sufficient yields to permit visualization in the electron density maps. Other factors, such as transient changes in the electric field in the active center gorge, rather than simply close proximity of the azide and alkyne groups, are required. Nevertheless, crystalline complexes with the TZ2 precursor and the TZ2/PA5 precursor pair were obtained, which provide atomic snapshots of the mode of binding of the two precursors in the AChE gorge prior to the cycloaddition reaction. These structures, complementary to those of the preformed TZ2PA5 complexes, point to potentially favorable versus unfavorable orientations of the TZ2 tacrine (1-azido-ethyl-2-amino-*N*′-9′-(1′,2′,3′4,′-tetrahydroacridinyl)) and PA5 phenanthridinium (3,8-diamino-5-oct-7′-ynyl-5-phenylphenanthridinium) moieties in the active site and the PAS, respectively, and reveal unexpected concerted swivel motions, mainly due to electrostatic influences of His447 in the active center, Tyr337 in the constricted region of the gorge, and Tyr341 at the gorge mouth, associated with binding of the TZ2 precursor.

EXPERIMENTAL PROCEDURES

Materials and Inhibition Studies. The TZ2, PA5 and PA6 precursors and the *anti* and *syn* TZ2PA5 and TZPA6 regioisomers, synthesized and purified as triflate and tosylate salts, respectively[15,16] (Scheme 1), were provided by Drs. Roman Manetsch and Antoni Krasiński (Skaggs Institute of Chemical Biology, The Scripps Research Institute, La Jolla, CA). Stock solutions of all but TZ2 in the 1−50 mM range in methanol or ethanol were titrated spectrophotometrically from absorbance of the phenyl-phenanthridinium moiety ($\varepsilon_{490\ nm}$ = 6000 M^{-1} cm^{-1}); they were stored in septum vials at −20 °C and manipulated on frozen racks.

Soluble mAChE expressed in HEK-293 cells[20] was purified by affinity chromatography with desorption using succinyldicholine and further processed and stored as described.[21] Inhibition constants were measured at 20 °C from the ratio of dissociation and association rates ascertained by conventional mixing and stopped-flow instrumentation as previously described[15,16,18,22] (Table 1).

DOI: 10.1021/jacs.5b11384
J. Am. Chem. Soc. 2016, 138, 1611−1621

Table 1. Kinetic Parameters for Inhibition of mAChE Enzymatic Activity

	TZ2PA5 isomers		TZ2PA6 isomers		precursors		framework inhibitors	
	syn[a]	*anti*[a]	*syn*[b]	*anti*[b]	TZ2[c]	PA5/PA6[c]	Tacrine[d]	Propidium[d]
ki (10^{10} M^{-1} min^{-1})	1.2	1.3	1.7	2.5	0.25	1.2	0.78	1.4
k−*i* (min^{-1})	0.028	0.43	0.007	0.22	58	4300	1.38	15000
K_i (pM)	2.3	33	0.4	8.9	23 × 10^3	360 × 10^3	18 × 10^3	1100 × 10^3

[a]From ref 16. [b]From ref 15. [c]From ref 17. [d]From ref 49.

Table 2. Summary of Soaking Experiments

mixture composition	ligand conc (μM)	soaking method #	bound ligand[a]	structure # in Table 3
TZ2PA6 *syn*	50	1 (4 °C)	TZ2PA6 syn[b]	
TZ2PA6 *anti*	50	1 (4 °C)	TZ2PA6 anti[b]	
TZ2PA5 *syn*	100	1 (4 °C)	TZ2PA5 syn[c]	1
TZ2PA5 *anti*	50/100/1000	1 (4 °C)	TZ2PA5 anti[c]	2
TZ2PA6 *syn* + *anti*	50 + 50	1 (4 °C)	TZ2PA6 syn[b]	
TZ2PA5 *syn* + *anti*	50 + 50	1 (4 °C)	TZ2PA5 syn[c]	3
TZ2PA5 *syn* + *anti*	50 + 300	1 (4 °C)	TZ2PA5 anti[c]	4
PA6	100	1 (4 °C)	none	
PA5	100	1 (4 °C)	none	
TZ2 + PA6	50 + 50/100	2 (4 °C)	TZ2[d]	
TZ2 + PA5	50 + 50/100	2 (4 °C)	TZ2[c]	5
TZ2 + PA6	50 + 200	3 (4 °C, sequential)	TZ2[d]	
TZ2 + PA5	50 + 200	3 (4 °C, sequential)	TZ2[d]	
TZ2 + PA6	100 + 1000	4 (20 °C, sequential)	TZ2[d]	
TZ2 + PA5	100 + 1000	4 (20 °C, sequential)	TZ2 + PA5[c]	6

[a]Upon inspection of the electron density for each data set, all were below 3.0 Å resolution and above 97% completeness. [b]Same ligand binding pose and mAChE side chain conformations as in the cocrystallized complexes.[18] [c]For X-ray data and refinement statistics, see the Experimental Section and Table 3. [d]Same result as for structure 5, but lower quality.

Preparation of the Crystalline Complexes and Data Collection. mAChE was crystallized at 4 °C in the presence of PEG550MME or PEG600 (25−35%) (v/v) in Hepes or sodium acetate 60−100 mM, pH 6.5−8.0.[21] The TZ2PA5 and TZ2PA6 complexes and expected PA5 and PA6 complexes were generated by soaking mAChE crystals in 20 μL sitting drops made of the well solution supplemented with PEG up to 35% (v/v) to ensure cryoprotection and with *anti*, *syn*, or both at 50 μM to 1 mM concentrations (4 °C, 24−36 h) (method 1) (Table 2). Attempts to achieve cycloaddition of the TZ2 and PA5/PA6 precursors in crystallo used either concomitant soaking with TZ2 50 μM and PA5/PA6 50−150 μM (4 °C, 24−48 h) (method 2); or sequential soaking with TZ2 50 μM (4 °C, 24 h), then a fresh mix of TZ2 50 μM and PA5/PA6 200 μM (4 °C, 24 h), followed by another fresh mix of the same (4 °C, 24 h) (method 3); or mAChE crystals grown at 4 °C and transferred to 20 °C (a procedure that led to no significant loss of diffraction for ca. 2 weeks, whereas no mAChE crystals could be obtained directly at 20 °C), for concomitant soaking with a mix of TZ2 100 μM and PA5/PA6 1 mM (20 °C, 24 h), then a fresh mix of the same (20 °C, 3 days), followed by another fresh mix of the same (20 °C, 2 h) (method 4). The use of concentrations greater than 1 mM was precluded by ligand solubility or crystal damage. The soaked crystals were directly flash-cooled in the nitrogen gas stream (100 K). Crystals belong to the orthorhombic space group $P2_12_12_1$ with unit cell dimensions a = 79.7 Å, b = 111.9 Å, c = 226.5 Å. Oscillation images were integrated with XDS,[23] and data were scaled and merged with SCALA.[24]

Structure Determination, Refinement and Analysis. The apo-mAChE structure (accession code 1J06[25]) without solvent was used as a starting model to refine the structures of the various mAChE complexes with the programs REFMAC[26] and autoBUSTER.[27] Rigid-body refinement was performed on each of the two subunits in the canonical crystalline dimer using all data followed by cycles of restrained refinements including NCS restraints and TLS refinement, with each subunit defining a TLS group. The molecular structures of the inhibitors and the associated topological and parametric data were generated with SKETCHER.[24] A random set of reflections (2%, 2255 reflections) taken from the succinyldicholine-mAChE complex structure (2HA2)[21] was set-aside for cross-validation purposes. In each case, the resulting sigmaA-weighted 2Fo−Fc and Fo−Fc electron density maps were used to position the inhibitor and correct the protein model with the graphics program COOT.[28] Data collection and refinement statistics are summarized in Table 3.

The reported six structures comprise residues Glu1-Ala541 and Glu4-Thr540 for the two respective mAChE molecules in the asymmetric unit and one to two well-ordered PEG molecule(s) trapped in the four-helix bundle.[25] High temperature factors and weak electron densities are associated with the short Ω loop Cys257-Cys272 and the surface loop region Asp491-Pro498. The stereochemistry of each structure was analyzed with MolProbity;[29] with the exception of the catalytic Ser203, no residues were found in the disallowed regions of the Ramachandran plot. The rmsd values between the structures of the *syn*- and *anti*-TZ2PA5-mAChE complexes and each of the *syn*- and *anti*-TZ2PA6-mAChE, TZ2+PA5-mAChE and TZ2-mAChE complexes are in the 0.16−0.33 Å range for 531 Cα atoms. The atomic coordinates and structure factors of the two *syn*- and *anti*-TZ2PA5 complexes obtained by standard soaking procedures (structures 1 and 2, respectively), the *syn*-TZ2PA5 complex obtained by soaking a 1:1 molar *syn* and *anti* mixture (structure 3), the *anti*-TZ2PA5 complex obtained by soaking a 1:6 molar *syn* and *anti* mixture (structure 4), the TZ2 complex obtained by soaking a 1:2 molar TZ2 and PA5 mixture (structure 5), and the TZ2+PA5 complex obtained by soaking a 1:10 molar TZ2 and PA5 mixture at 20 °C (structure 6), have been deposited with the Protein Data Bank (cf. Table 3 for accession codes). Analysis of cavities and mouth openings in mAChE was carried out using CASTp.[30] Figures 1 and 2 were generated with PyMOL.[31]

RESULTS AND DISCUSSION

Kinetic parameters recorded in solution for binding of the TZ2PA5 regioisomers to mAChE led to similar association rates (*ki*) but a ∼15-fold greater dissociation rate (*k*−*i*) for the

DOI: 10.1021/jacs.5b11384
J. Am. Chem. Soc. 2016, 138, 1611−1621

Table 3. Data Collection and Refinement Statistics for the TZ2PA5- and TZ2/PA5-mAChE Complexes

	TZ2PA5 isomers				precursors	
soaked ligand	*syn*	*anti*	*syn* + *anti*		TZ2 + PA5	
soaked concentration (μM)	100	100	50 + 50	50 + 300	50 + 100	100 + 1000
soaking method # (cf. Table 2)	1	1	1	1	2	4
bound ligand in structure	*syn*	*anti*	*syn*	*anti*	TZ2	TZ2 + PA5
structure # (panel in Figure 1)	1 (B left)	2 (B right)	3 (C left)	4 (C right)	5 (D left)	6 (D right)
Data collection[a]						
beamline (ESRF)	ID14-EH2	ID23	ID14-EH1	ID14-EH1	ID14-EH3	ID14-EH3
wavelength (Å)	0.933	0.953	0.931	0.931	0.931	0.931
resolution range (Å)	45−2.6	46−2.5	44−2.5	45−2.7	46−2.1	46−2.7
total observations	258168	317810	343486	231741	759812	337190
unique reflections	62667	71018	69707	56257	115553	56558
multiplicity	4.1 (4.1)	4.5 (4.2)	4.9 (5.0)	4.1 (4.2)	6.6 (6.2)	6.0 (6.1)
completeness (%)	98.9 (99.7)	99.3 (96.3)	99.7 (99.7)	99.6 (99.8)	96.6 (84.4)	99.6 (99.4)
$I/\sigma(I)$	18.7 (3.3)	17.8 (3.0)	21.6 (3.1)	16.9 (3.2)	22.7 (3.6)	12.1 (3.2)
R_{sym}[b]	6.9 (56.5)	5.7 (60.1)	7.2 (68.8)	7.9 (60.6)	5.5 (59.7)	11.3 (63.5)
B Wilson plot (Å^2)	59.5	61.8	55.9	62.9	37.8	59.4
Refinement[c]						
R-factor/(%)	18.2 (21.8)	19.1 (24.4)	17.6 (21.5)	17.6 (21.8)	17.6 (21.1)	17.5 (21.4)
R-free (%)	20.3 (24.9)	21.5 (30.9)	19.7 (24.8)	20.8 (24.4)	19.3 (20.7)	20.2 (26.0)
r.m.s.d.[d]						
bonds (Å)/angles (deg)	0.01/1.1	0.01/1.1	0.01/1.12	0.01/1.1	0.01/1.05	0.01/1.1
Mean B-factors (Å^2)						
main/side chains	50.1/54.6	64.9/69.0	51.2/55.3	51.1/55.4	47.2/51.6	48.6/52.9
solvent/carbohydrate	46.8/84.7	54.3/126.2	49.4/98.9	45.3/106.2	53.3/104.5	44.3/−
ligand/PEG[e]	58.7/62.0	81.7/79.0	60.8/69.6	75.2/63.2	56.6/76.3	63.9/71.9
PDB accession code	5EHN	5EHQ	5EHZ	5EIA	5EIE	5EIH

[a]Values in parentheses are those for the last shell. [b]$R_{sym} = |I - \langle I\rangle|/\Sigma I$, where I is an individual reflection measurement and $\langle I\rangle$ is the mean intensity for symmetry-related reflections. [c]R-factor = Σ ||Fo| − |Fc||/Σ |Fo|, where Fo and Fc are observed and calculated structure factors, respectively. R-free is calculated for 2% of randomly selected reflections excluded from refinement. [d]Root-mean-square deviations from ideal values. [e]PEG molecules trapped at the four-helix bundle.[25]

anti compared to the *syn*, a difference fully reflected in the equilibrium dissociation constants, K_i (Table 1).[16] These values, similar to those obtained for the previously described TZ2PA6 congeners, further highlight the stereoelectronic preferences inside the AChE gorge for efficient enhancement of the cycloaddition reaction into a *syn* product, as also observed from molecular dynamics simulations.[32,33] Yet, in contrast to our initial expectation, these values also point to a limited influence of alkyl chain shortening by one C−C bond, from C6 to C5. Finally, comparing the behavior of the two precursors, TZ2 and PA5, with that of the framework inhibitors, tacrine and propidium, reveals that adding the aliphatic azide and the alkyne moieties has little influence on association rates but accelerates (tacrine) or retards (propidium) dissociation.

To document the structural bases for the affinity differences between (i) the *syn* and *anti* TZ2PA5 isomers and (ii) the TZ2PA5 and TZ2PA6 inhibitors toward mAChE, we solved crystal structures of the two TZ2PA5 complexes and analyzed them comparatively and with previous structures of the *syn* and *anti* TZ2PA6 complexes.[22] Since the former were obtained by crystal soaking and the latter by cocrystallization, to ascertain adequacy of the comparison we also analyzed structures of *syn* and *anti* TZ2PA6 complexes obtained by crystal soaking (Tables 2 and 3). Moreover, to explore whether the cycloaddition reaction could occur in crystallo and form the triazole at higher yields to those obtained in solution,[15] we attempted to favor the trapping of properly oriented precursors and efficient reactant ligation within the crystalline mAChE gorge. To this end, we designed soaking procedures involving significant molar excesses of each inhibitor over both mAChE and the K_i value for complex formation; unbalanced inhibitor concentration ratios to compensate for the lower affinity of the *anti* versus *syn* isomers and PA5/PA6 versus TZ2 precursors; soaking of TZ2 first to form an active site-anchored bait for any PA5/PA6 precursor binding the PAS; transfer and soaking at 20 °C of crystals grown at 4 °C; and long incubation times and replenished soaking solutions (see Experimental Procedures and Table 2). X-ray data within the 2.1−2.7 Å resolution range and above 97% completeness were collected from all soaked crystals and solved, and the electron density map issued from each data set was carefully inspected for presence of the bound ligand(s) (Table 3). Since several data sets led to equivalent interpretations, only those structures with optimal crystallographic parameters are described below.

***syn*- and *anti*-TZ2PA5 Complexes Obtained from Standard Soaks (Structures 1 and 2).** The crystal structures of the *syn*- and *anti*-TZ2PA5-mAChE complexes show well-ordered and tightly bound inhibitor molecules spanning the full length of the gorge (see Experimental Procedures) (Figure 1A,B). As originally found for the *syn*- and *anti*-TZ2PA6-mAChE complexes, the TZPA generic binding site encompasses three discrete loci: (i) the active center at the base of the gorge where the tricyclic tetrahydro acridine moiety nestles; (ii) an intervening site in the constricted region within the gorge that associates with the triazole moiety and adjacent methylene group extensions; (iii) the PAS at the gorge rim where the phenyl-phenanthridinium moiety binds (Figure 1B).[18] In fact,

DOI: 10.1021/jacs.5b11384
J. Am. Chem. Soc. 2016, 138, 1611−1621

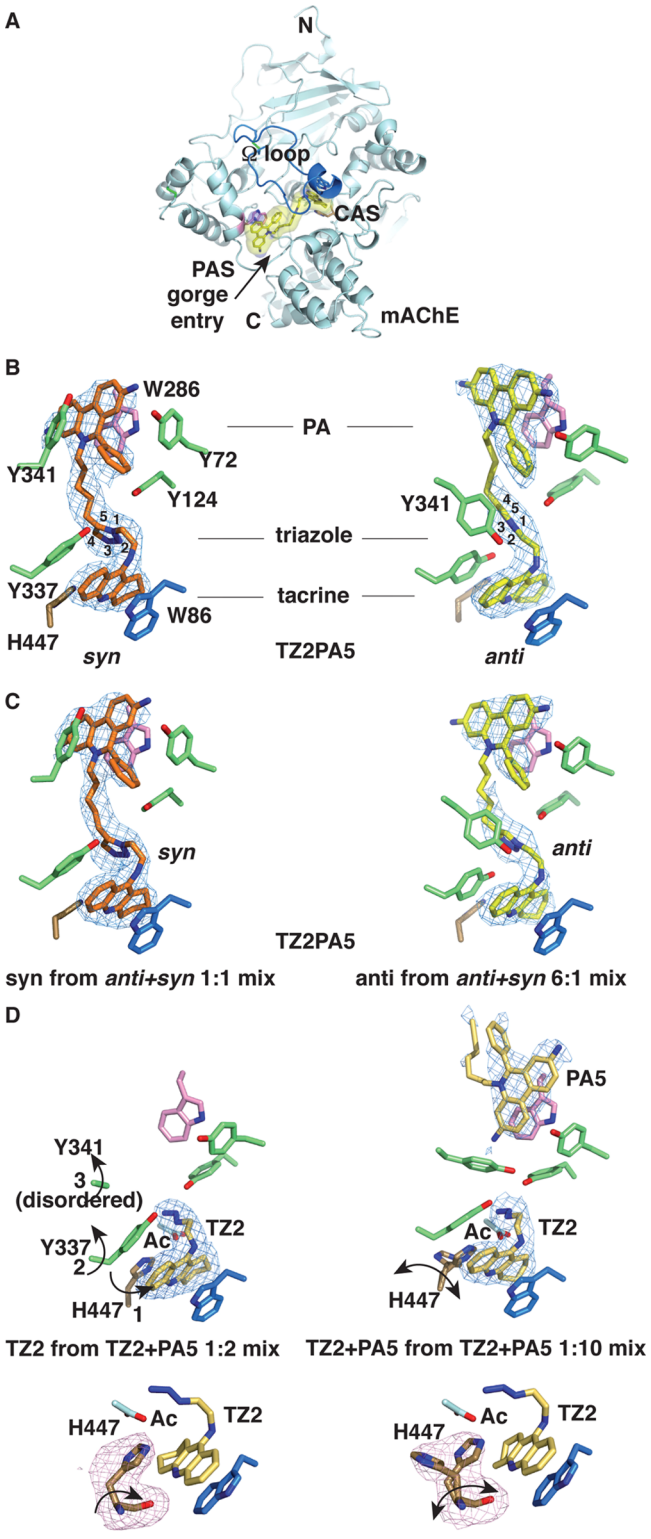

Figure 1. Overall view of the mAChE subunit and close-up views of the bound ligands in the six crystalline complexes. (A) The mAChE molecule (cyan ribbon) is viewed down the active site gorge with the *anti* TZ2PA5 isomer (yellow bonds and transparent molecular surface) bound within the gorge. The catalytic triad residues Ser203, Glu334 and His447 are displayed in orange at the center of the subunit. The long Ω loop Cys69-Cys96 is highlighted in blue, PAS residue Trp286 is in pink and Trp86 at the base of the gorge in marine. The three disulfide bridges respectively located in the long Ω loop, in the short Ω loop Cys257-Cys272, and between helix α(4)7,8 and the C-terminal helix α10, are displayed as green bonds. (B) mAChE-bound *syn* and *anti* TZ2PA5 isomers resulting from individual soaks at 4 °C (orange and yellow bonds, respectively, with blue nitrogens and numbered triazole atoms) (structures 1 and 2, see Tables 2 and 3). (C) mAChE-bound *syn* and *anti* TZ2PA5 isomers resulting from mixed soaks of *syn* and *anti* at 1:1 and 1:6 molar ratios, respectively, at 4 °C (same color codes as in panel B) (structures 3 and 4). (D) mAChE-bound TZ2 resulting from a soak of TZ2 and PA5 at a 1:2 molar ratio and at 4 °C (left, structure 5) and mAChE-bound TZ2 and PA5 resulting from a soak of TZ2 and PA5 at a 1:10 molar ratio and at 20 °C (right, structure 6), both showing a bound acetate (white) (same color codes as in panels B and C). The Fo−Fc omit maps in the 2.7−2.1 Å resolution range contoured at 2.5 or 3σ (cyan) are displayed for each bound ligand, and for the catalytic His447 side chain in the close-up views underneath. The mAChE side chains that interact with the tacrine, triazole and phenanthridinium moieties of the isomers or precursors are colored blue, green and violet, respectively, with blue nitrogens and red oxygens. The coordinated side chain motions of the catalytic His447 (brown), Tyr337 and Tyr341 upon TZ2 binding are numbered and indicated by curved arrows. Proximity of the terminal azide and new flipped His447 seems to favor anchoring of an acetate molecule at proximity of the Ser203 hydroxyl in the oxyanion hole.

the main difference between the two complexes resides in the position of the *syn*-TZ2PA5 phenanthridinium ring, that retains a similar orientation as that of the *anti* isomer but is shifted by ∼2 Å toward the bottom of the gorge to obey a similar centroid-to-centroid separation distance (∼2.4 Å) of the *syn versus anti*-substituted triazole midway in the gorge (Figures 2A and 3).

Compared to the *syn*-TZ2PA6 complex, the *syn*-TZ2PA5 complex reveals no significant differences in the inhibitor and AChE conformations at the base and in the region of constriction of the gorge. However, at the PAS, the *syn*-TZ2PA5 phenanthridinium ring adopts a perpendicular orientation compared to that of the *syn*-TZ2PA6 congener, due to the shorter alkyl chain being unable to avoid steric clashes between the phenyl group and the Asp74 and Tyr341 side chains appended to the gorge wall (Figures 1B and 2A). In turn, the newly positioned phenanthridinium ring dislodges the Tyr341 phenol ring from the PAS surface into the solvent through a large ∼90° arc movement associated with backbone displacements of the residue pair Tyr341-Gly342. These large conformational rearrangements at the PAS are associated with a 60° arc movement of the neighboring Tyr337 phenol in the constricted region as previously observed for *syn*-TZ2PA6. In this new orientation, the solvent-exposed Tyr341 side chain aligns nearly parallel to the phenanthridinium ring to create a sandwich of π orbitals with the Trp286 side chain, a configuration reminiscent of intercalation of the *syn*-TZ2PA6 between the Tyr72 phenol ring and a dislodged Trp286 indole ring at the PAS.[18]

Compared to the *anti*-TZ2PA6 complex, the *anti*-TZ2PA5 complex shows no significant conformational changes in the position/orientation of mAChE side chains at the entrance of and within the gorge, while minor differences only are observed in the overall conformation and binding pose of the inhibitor, with a ∼ 0.7 Å drift of the triazole toward the mouth of the

DOI: 10.1021/jacs.5b11384
J. Am. Chem. Soc. 2016, 138, 1611−1621

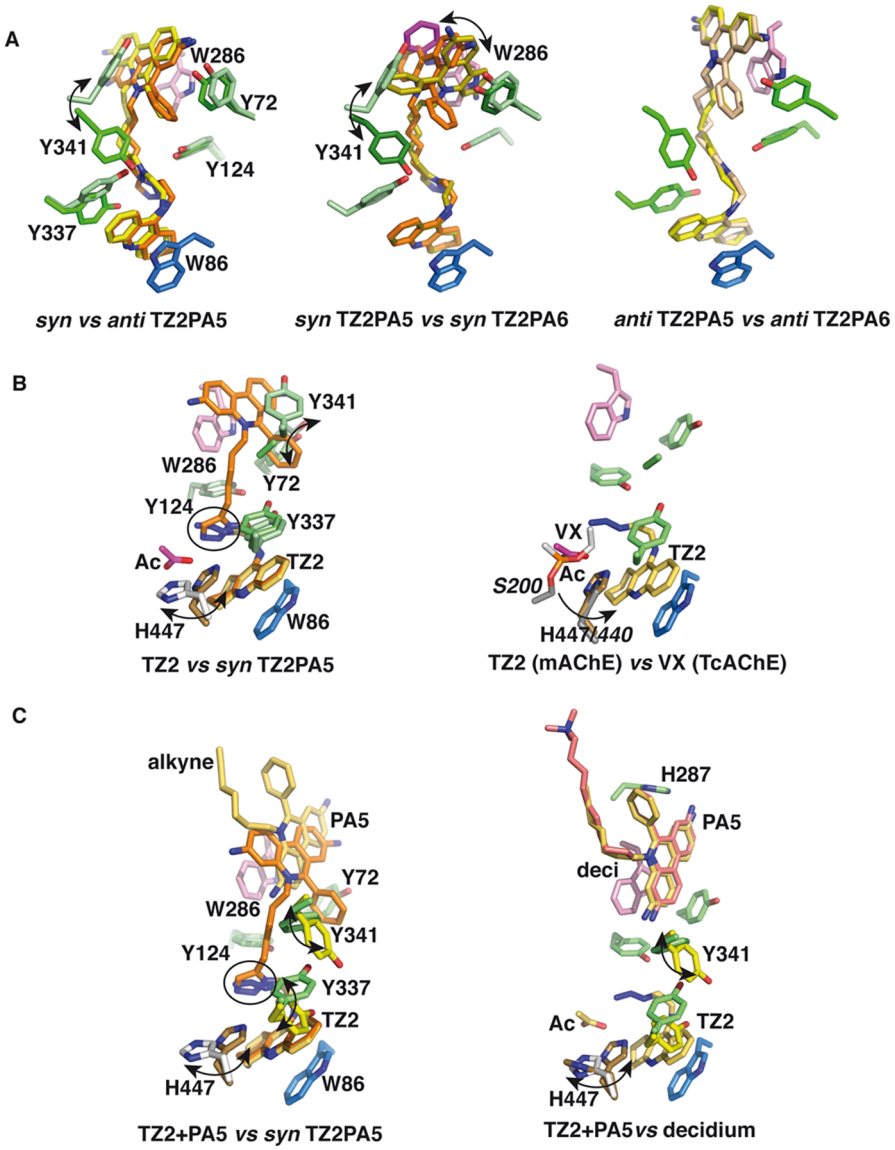

Figure 2. Comparative analysis of representative crystalline complexes. (A) Superimposed overall views of (from left to right as labeled) the *syn* (orange bonds) and *anti* (yellow bonds) TZ2PA5 isomers; the *syn* TZ2PA5 (orange) and *syn* TZ2PA6 (light orange, accession code 1Q83) isomers; and the *anti* TZ2PA5 (yellow) and *anti* TZ2PA6 (light yellow, accession code 1Q84) isomers, all bound to mAChE. (B) Superimposed overall views of (from left to right as labeled) the TZ2 precursor (light yellow) with acetate (pink) and the *syn* TZ2PA5 isomer (orange), all bound to mAChE; and the TZ2 precursor bound to mAChE (light yellow) and the organophosphate inhibitor VX in the pro-aged conjugate with TcAChE active site Ser (white bonds for VX and grey bonds for TcAChE Ser200 and His440, accession code 1VXR). The phosphonyl oxygen in TcAChE-bound VX points back and overlaps with the position of one of the oxygens in mAChE-bound acetate. (C) Superimposed overall views of (from left to right as labeled) the TZ2+PA5 precursors (light yellow) and the *syn* TZ2PA5 (orange), or the bifunctional inhibitor decidium (salmon, accession code 1J07), all bound to mAChE. The encircled region in the left B/C panels points to the mimicry of the azide moiety in TZ2 and the triazole nitrogen atom of *syn* TZ2PA5 in their respective mAChE complexes. The Trp286, Tyr341 and His447 side chains (in magenta, green and brown, respectively) are distinctively positioned in the complexes, as highlighted by the curved arrows. Superimpositions were made according to all Cα atoms in the mAChE or TcAChE subunits.

gorge (Figures 1B and 2A). Here, the shorter alkyl chain has insignificant impact on the position and orientation of the phenanthridinium ring at the PAS, which adopts a parallel stacking interaction against the Trp286 indole ring similar to that found in the propidium complex.[25] However, a dimethylene segment of the *anti*-TZ2PA5 pentamethylene chain connecting the triazole to the phenanthridinium ring is not clearly visible in the electron density maps, suggesting that a shorter alkyl chain in the *anti* isomer is slightly less conformable to the shape of the gorge wall.

We previously proposed that distinct positions and orientations of the triazole in the constricted region of the gorge between the *anti* and *syn* TZ2PA6 isomers, corresponding to a ~1.5 Å drift of the *syn*-triazole toward the base of the gorge, govern the phenanthridinium position at the PAS. Such positioning could be also responsible for the expulsion of the Trp286 indole from the PAS surface.[18] Hence, deletion of a methylene in the alkyl chain linking the phenanthridinium ring to the triazole in the TZ2PA5 or TA2PZ5 congener was expected to result in a switch to the *anti* binding pose at the PAS with the linker extended by ~1.5 Å.[16] In fact, a shorter

DOI: 10.1021/jacs.5b11384
J. Am. Chem. Soc. 2016, 138, 1611−1621

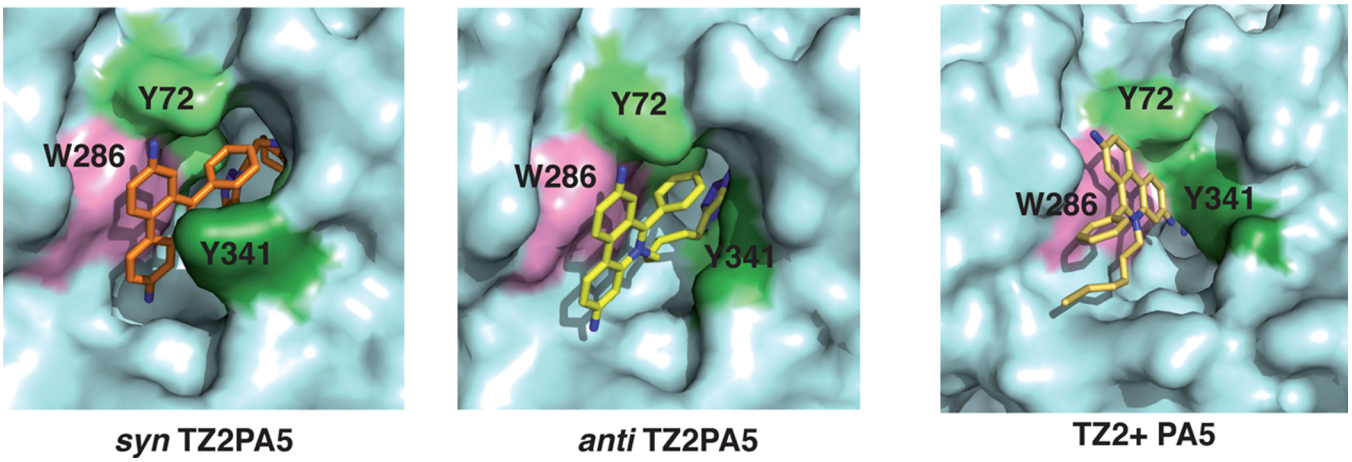

Figure 3. Distinctive topographies of the PAS regions in the *syn* TZ2PA5, *anti* TZ2PA5 and TZ2+PA5-mAChE complexes. Views (looking down the active site gorge) of the PAS region of mAChE occupied by the phenyl-phenanthridinium moiety present in the (left) *syn* TZ2PA5 isomer, (middle) *anti* TZ2PA5 isomer and (right) TZ2+PA5 pair of precursors (same color codes as in Figures 1 and 2). The mAChE molecular surfaces buried to a 1.4 Å radius probe at the complex interfaces are shown in light blue and the Trp286, Tyr72 and Tyr341 side chains at the PAS are highlighted in pink, green and dark green, respectively. The gorge mouth openings based on the solvent-accessible surface for the *syn* and *anti* complexes are 32 $Å^2$ and 24 $Å^2$, corresponding to circumferences of 49 Å and 27 Å, respectively (to be compared with 20 $Å^2$ and 29 Å, respectively, for apo mAChE) (averaged values over the two subunits in the mAChE dimer). In the TZ2+PA5 complex the gorge path is partially occluded.

spanning distance between the phenanthridinium ring and the triazole causes the Tyr341 phenol ring to be dislodged from the PAS surface associated with a minor conformational adjustment of the facing Tyr72 side chain at the gorge rim.

This comparative analysis confirms that when compared to TZ2PA6, shortening the alkyl chain by one carbon bond does not favor intercalation of the phenanthridinium ring between Trp286 and Tyr72, as seen for the related *syn*- and *anti*-TZ2PA6 with the Trp286 side chain dislodged from the PAS surface in mAChE and the Y337A mutant.[18,19] Instead, shortening the length of the alkyl chain generates a swinging movement of the Tyr341 phenol ring across the gorge entry, a rotational movement not seen in previous mAChE and TcAChE complexes (Figure 3). Together with the previously observed large movement of the Trp286 side chain, we provide new evidence for positional flexibility of aromatic side chains at the PAS, supporting rapid breathing motions of the gorge entrance to facilitate access of incoming substrate to the active site at the gorge base.[34]

The enhanced sensitivity and reliability of the in situ click chemistry approach has enabled us to detect an inverted triazole orientation in two, *syn*-TA2PZ6 and *syn*-TA2PZ5, out of the three new compounds, resulting from the alternative synthesis using the TA2/TZ2 and PZ5/PZ6 pair of precursors.[16] Compared to the original high affinity ligands, i.e., the *syn*-TZ2PA6 (410 fM for mAChE) and *syn*-TZ2PA5 (2300 fM) products, inhibitors harboring an inverted triazole confer the same binding energy with dissociation constants of 610 fM and 3000 fM for the *syn*-TA2PZ6 and *syn*-TA2PZ5, respectively. Hence, inversion of the triazole orientation shows a less pronounced influence on binding affinity, when compared to the critical, polarity-dependent position of the triazole centroid within the gorge (e.g., TZ6PA2/TZ5PA2 not formed in situ).

***syn*- and *anti*-TZ2PA5 Complexes Obtained from *syn*/*anti* Mixtures (Structures 3 and 4).** Considering the preferred formation of a *syn* isomer upon the cycloaddition reaction, we wondered whether crystalline mAChE would also select this *syn* isomer from mixtures of preformed *syn* and *anti*. Soaking mAChE crystals with an equimolar mixture of the *syn* and *anti* TZ2PA5/PA6 isomers led to a tightly bound *syn* isomer but no evidence (i.e., occupancy below ~30%) for a bound *anti* isomer, a feature consistent with the difference in binding affinity of the two congeners (Figure 1C, Tables 1 and 2). The phenanthridinium ring in bound *syn* is in a virtually identical position as in the *syn*-TZ2PA5 complex in structure 1, and the bound inhibitor shares a similar conformation and network of interactions with mAChE. This observation slightly differs from our previous observation of a predominant *syn* isomer and low abundance *anti* isomer trapped in the crystalline Tyr337Ala mutant of mAChE soaked with an equimolar mix of *anti* and *syn* TZ2PA6.[19] The 400 to 8000-fold lower K_d values and 3 to 4-fold lower *anti*/*syn* K_d ratio of the TZ2PA6 regioisomers for the mAChE mutant, compared with those of the TZ2PA5/PA6 isomers for wild-type mAChE, are governed by slower dissociation rates, since association rates approach the diffusion limit. Thus, as equilibrium is approached, dissociation rates likely account for the different ratios of occupation. Nevertheless, soaking mAChE crystals into an unbalanced, 1:6 mixture of the *syn* and *anti* isomers resulted in a tightly bound *anti* isomer in virtually identical position to that seen in the *anti*-TZ2PA5 complex formed using only the anti isomer, with no trace of a bound *syn* isomer (Figure 1C). Hence, despite the similar association rates of the two regioisomers, the 15-fold difference in their dissociation rates provided a sufficient interval to select the higher affinity complex during the time frame of the soaking procedure.

TZ2- and TZ2/PA5-mAChE Complexes Obtained from TZ2/PA5 Mixtures (Structures 5 and 6). In situ click chemistry offers an elegant approach for identifying ligand building blocks from a diverse library using an optimum combination of azide and alkyne pairs from a library of each structure,[15] but the efficiency in triazole formation remains the rate limiting step, with a short-lived transition state resembling the promotion of the cycloaddition.[14] To provide snapshots of the cycloaddition process prior to product ligation and explore the potential of the click reaction to occur within crystalline AChE, we soaked mAChE crystals with various molar ratios of

DOI: 10.1021/jacs.5b11384
J. Am. Chem. Soc. 2016, 138, 1611−1621

the TZ2 and PA5/PA6 precursors at concentrations up to 3 orders of magnitude over their K_i (Table 1) and employed protocols expected to favor ligand binding and cycloaddition (Table 2).

Soaking PA5/PA6 at a concentration 2 orders of magnitude greater than the K_i value led to mAChE structures devoid of a bound ligand at the PAS (Table 2) as previously observed while trying to soak the framework inhibitor, propidium, or its higher affinity congener, decidium, into mAChE crystals[25] (Table 1). Soaking the TZ2 and PA5/PA6 precursors together at a 1:2 molar ratio (method 2, see Experimental Procedures) led to a tightly bound TZ2 at the gorge base near the catalytic triad, but again no trace of a bound PA5/PA6 at the PAS (Table 2; Figure 1D). The TZ2 tricyclic tetrahydroacridine moiety retains the same binding pose as observed for the bound *anti*- and *syn*-TZ2PA5/PA6 products (Figure 2B). The terminal azide group lies in the vicinity of the oxyanion hole, in which an acetate molecule (from the crystallization liquor) is bound, within 4 Å of the Gly122 nitrogen and 5.4 Å to the Ser203 hydroxyl and is firmly stabilized by the Tyr124 hydroxyl. This position of bound TZ2 may reflect its position during the *syn* cycloaddition reaction, i.e., with the azide and alkyne extended in a parallel, rather than antiparallel, orientation for the formation of the favored *syn*-triazole product, as previously predicted by molecular dynamics calculations.[15,32] Hence, the TZ2 dimethylene chain adopts a hook shaped conformation that positions the terminal azide to match (within 1 Å) the nitrogen atoms of the *syn*-triazole in the mAChE-TZ2PA5 complex. In contrast, the terminal azide is remote by more than 2 Å from the corresponding nitrogen atoms in the *anti*-triazole. Most unexpectedly, the bound TZ2 precursor appears to disrupt the catalytic triad and its associated hydrogen bonding, since the catalytic His447 side chain swivels by ∼180° in the plane of the ring with no alternative partner for hydrogen bonding, leading to catalytically nonproductive side chain orientations in the triad. Yet, the productive conformation of His447 does not appear to clash sterically with the tacrine moiety of the TZ2 precursor. Such conformational mobility of His447 was not observed in the tacrine-TcAChE complex,[35] the TZ2PA5/PA6-mAChE complexes (Figure 1B, and Figure 2 in ref 18) nor previous mAChE structures with a bound acetate,[19,21,25] but it resembles the uncoupling movement of catalytic His440 observed in the pro-aged VX conjugate with TcAChE active site Ser200,[36] (Figure 2B) and in various organophosphate conjugates of mAChE.[37a,b]

Conformational mobility of His447 may also reflect its inherent dynamic behavior, independent of the reversible movement observed upon dephosphonylation of the AChE-organophosphate conjugate or of that described for the active site His residue of acyl-enzymes of the trypsin family.[36,38] In absence of a bound PA5/PA6 at the PAS, the His447 rotation is accompanied by a similar motion of the Tyr337 phenol in the constricted region as seen in *syn*-TZ2PA5/PA6-bound mAChE, leading to high disorder of the Tyr341 side chain at the PAS. Hence, binding of the TZ2 precursor at the base of the gorge appears to orchestrate coordinated side chain motions lining the inner wall of the gorge path to generate a *syn*-triazole regioisomer.

The use of higher molar ratios and/or higher concentrations of the TZ2 and PA5/PA6 precursors along with sequential soaks (method 3) or a temperature increase (method 4) again led to tightly associated TZ2 moieties at the gorge base and no bound PA5/PA6 at the PAS (Table 2), except in one data set where the two intact azide and alkyne precursors were found (Figures 1D and 2C). In this structure, bound TZ2 adopts a similar position and conformation as in the TZ2-mAChE complex, a feature supporting strong intermolecular stabilization at the base of the gorge, while a partially disrupted catalytic triad with an alternate conformation of His447 is observed, as also seen in the TZ2-mAChE complex. At the PAS, bound PA5 displays partial occupancy only, a feature likely to reflect the 15-fold difference in the binding affinities of the two precursors for mAChE in solution despite the use of unbalanced concentrations and/or an unfavorable binding orientation. Compared to its position in bound *anti*-TZ2PA5/PA6, the PA5 cationic phenanthridinium ring retains a near-parallel stacking with the Trp286 indole through a $\pi-\pi$ interaction, but it is rotated by ∼180° around its centroid axis, an orientation reminiscent to that of the related inhibitors, decidium and propidium, bound to crystalline mAChE[25] (Figure 2C). As a result, the phenanthridinium ring of the PA5 precursor undergoes stabilizing polar interactions with the His287 imidazole instead of the Gln291-Ser293 side chains across the gorge entry as seen in the TZ2PA5-complex, while the phenol group of Tyr341 is shifted by ∼45° outward, leading to a partial occlusion of the gorge path (Figure 3). In turn, the protruding pentamethylene unit bearing the alkyne group projects toward the solvent where it is partially disordered (i.e., only partially visible in the electron density maps) instead of occupying the gorge path as required for the cycloaddition reaction in situ (Figure 1D), and displaces three of the ordered water molecules observed in the structure of *syn* TZ2PA5 complex. In fact, this nonproductive orientation of the linker for cyclization is reminiscent of that of the 10-carbon alkyl chain of mAChE-bound decidium, found to lie at the subunit surface instead of within the gorge despite crystallization of a fully inactive complex formed in solution.[25] It is also consistent with the highest energy conformation of the PA6 alkyne chain found upon in silico docking of the TZ2/PA6 pair to AChE, suggesting a low energy requirement for alkyl chain entering and residing in the dynamically constrained crystalline protein.[33] At the level where the triazole should form upon cycloaddition within the gorge, the positioning of the partially ordered Tyr341 side chain, midway in its positions in the *anti*/*syn*-TZ2PA6 and *syn*-TZ2PA5 complexes, and the coordinated arc motion of the Tyr337 side chain indicate that coupled interactions rather than random dynamic fluctuations are necessary to favor alkyl chain entry into the gorge.

Implications of the Structural Data for Dynamic Combinatorial X-ray Crystallography. The key feature for the success of the "in situ click chemistry" approach is the simultaneous presence and proper orientation of the building blocks at their respective sites to enable apposition and ultimately cyclization of the alkyne in a parallel or antiparallel fashion. To date, detection of ligands reacted in crystallo from a mixture of precursors has been reported for imine-based reactions such as oxime/hydrazine formation, but only once for the Huisgen cycloaddition.[39−41] In one case, an oxindole-based inhibitor generated by hydrazone chemistry was found within crystals of cyclin-dependent kinase 2 exposed to a dynamic combinatorial library of precursors.[39] In the other case, well-ordered self-assembled benzamidine-derived products formed from a similar imine reaction of an aldehyde with a primary amine were visualized in the active site of trypsin using time-resolved crystallography.[40] In fact, the poor reactivity of oxime ligations at neutral pH values limits their use for biological applications, but it can be significantly accelerated by using

DOI: 10.1021/jacs.5b11384
J. Am. Chem. Soc. 2016, 138, 1611−1621

aniline as a nucleophilic catalyst, as demonstrated with trypsin crystals where an aniline-bound transition intermediate could be trapped.[40,42] These two studies, which promote imine-based over triazole-based ligation for in crystallo click chemistry, demonstrate that a crystalline protein bound with an anchor molecule not only functions as a solid state, reaction vessel for chemical ligation but also serves as a platform to generate more potent self-assembled products.[40] However, aniline-catalyzed imine formation requires active site accessibility and ability to accommodate a selective ternary complex involving an anchor molecule, aniline and a tuning molecule, two parameters not encountered with the buried active site gorge of AChE. Moreover, the precise location of the reactive aldehyde groups in the building blocks and the chemical nature of the linker clearly influence the efficiency of the ligation reaction and the binding affinity between protein and ligand.[40] This is particularly relevant for the Huisgen cycloaddition reaction, since two anchor points were essential for stabilizing each of the two reactants to achieve inhibitor formation in the crystalline state of carbonic anhydrase II.[41] Other amino functionalities have been studied to overcome the instability of imines produced from primary amines. Among those, reversible acylhydrazone connections between hydrazide and aldehyde building blocks were generated and screened toward inhibition of TmAChE, leading to a very potent bis-pyridinium inhibitor.[43]

For the 1,3-dipolar cycloaddition to take place in AChE, the high affinity tacrine building block should first bind to the base of the AChE active center gorge (as does the anchoring molecule in the active site of trypsin crystals),[40] and then be positioned for the complementary phenanthridinium building block to bind, a process that we tried to favor by using a *sequential* soaking procedure. The lowest energy state of the ternary complex would represent a snapshot of the building blocks prior to the cycloaddition reaction and therefore should give an indication of the reaction path that gives the favored triazole regioisomer. Effective catalysis of the cycloaddition inside the AChE gorge is dependent on very strict, parallel or antiparallel geometries and stereoelectronic appositions, as shown for the preferred *anti*-TZ2PA6 isomer for inhibition of *Drosophila* AChE.[44] A reversal of regioselectivity toward the *anti* isomer or a regioisomeric mixture (after 9 and 30 days of incubation, respectively) was also observed with new potent huprine-based inhibitors generated by in situ 1,3-dipolar cycloaddition in mouse or human AChE.[45]

Two factors are important to achieve the requisite affinity, selectivity and rate acceleration of the in situ cycloaddition, and our study provides initial evidence for achieving an ideal scenario. First, triazole formation requires that the azide and alkyne react in a parallel rather than antiparallel fashion causing the bond distance between tetrahydroacridine and phenanthridium be foreshortened by ∼1.2−1.4 Å. Transient changes in the local electric field alignments[46] upon binding of the precursors are also likely to govern rates of the azide−alkyne cycloaddition reactions as the triazole confers a strong dipole moment requiring a transition state resembling the product. A hydrogen-bonding network[47] and transient dipole formation within the active center gorge may facilitate the dynamic processes in solution. The tacrine moiety binds in the choline subsite in apposition with the indole of Trp86 and the aliphatic azide chain loops around to form a semicircle hook in the gorge associated with conformational motion of the His447 side chain in the active center, as observed in the TZ2-mAChE and TZ2/PA5-mAChE structures. In this regard, the inverted orientation of tetrahydroacridine in the *anti*-TZ2PA6 bound to the mAChE Tyr337Ala mutant may lead to an unfavorable antiparallel configuration of the terminal azide−alkyne groups.[19]

Second, accommodation and positioning of the phenanthridinium with an optimal alkyl-chain length also requires flexibility in side chain conformations, in particular those of Trp286 and Tyr341 at the rim of the gorge, but also that of Tyr337, found midway in the gorge. The conformational freedom observed for the phenanthridinium ring at the PAS compared to the more rigid tacrine at the bottom of the gorge, coupled to the side chain reorientations along the gorge path, may account for the time required by the AChE molecule to generate sufficient triazole product for ensuring detection in the electron density map. In fact, the structure of mAChE with the bound pair of precursors (structure 6) exemplifies this rate-limiting step. Comparative analysis of these structures reveals that at least four ordered water molecules are displaced in the upper part of the gorge to accommodate the *syn* TZ2PA5, suggesting that partial desolvation of the gorge could represent a rate-determining step during precursor binding kinetics. Identification of other motifs with a higher affinity and/or more straightforward binding pose than the phenanthridinium as candidate PAS ligands during the in situ click chemistry approach, such as phenyltetrahydroisoquinoline that was not previously known to bind the PAS of an AChE, may reduce conformational freedom and enhance ligation rates.[17] In this context, the unprecedented positioning in the upper part of the gorge of human AChE of the triazole formed from huprine azides and phenyltetrahydroisoquinoline alkynes clearly extends the potential of the in situ click chemistry for the design of new AChE inhibitors.[45]

Other chemical reactions such as conjugation of tetrahedral organophosphates at the active center Ser203 residue and oxime-reactivation of organophosphate-mAChE adducts have been performed successfully in crystalline mAChE[37a,c]. However, these reactions take place in the active site pocket and vicinal oxyanion hole, whereas the azide−alkyne reaction conducted in the AChE gorge is removed from and independent of the active site serine: rather, it is facilitated by the protein surface of the gorge, serving as a template and sequestering the reactants in a localized reaction volume. Similarly, in the nicotinic acetylcholine receptor that has no catalytic function, reaction between site-directed azides and alkynes occurs in the pocket located at the subunit interface and partially capped by loop C.[48]

In conclusion, compared with the PA6 precursor, the shorter alkyl chain of the alkyne-terminated PA5 precursor induces new conformational rearrangements involving the Tyr341 side chain at the mAChE PAS. Structural snapshots of precursors bound in the active site and at the PAS prior to cycloaddition and product formation clearly picture the preferred parallel orientation of the azide and alkyne reactant chains leading to preferred generation of a *syn* product, and unveil a coordinated cascade of side chain positional changes (Tyr337, Tyr341, His447) initiated by a disrupted catalytic triad, not observed in the mAChE complexes with the bound products nor the TcAChE-tacrine complex. These snapshots also strongly suggest that formation of the freeze-frame inhibitors can be driven by the proximity of the azide and alkyne reactants from a ternary complex of low fractional abundance and its residence time, of a few microseconds, in the framework of transient electric fields formed by the side chains within the gorge. By

DOI: 10.1021/jacs.5b11384
J. Am. Chem. Soc. 2016, 138, 1611−1621

employing various ligand concentrations and molar ratios, sequential addition of precursors, and a thermal energy increase during the soaking procedure, we have obtained original complexes revealing conformational features central to in situ click chemistry, yet we have not found appreciable evidence for appreciable cycloaddition in crystallo. The fraction of bound PA5/PA6 with the reactive azide properly positioned may be not sufficient for generating the electronic coupling for the biorthogonal reactions. A substantial electric field dipole passing briefly through the constricted region in the gorge may serve to diminish the required activation energies to form stronger dipoles of 4.7 D for *anti* triazoles and 5.2 D for *syn* triazoles.[50] It is also quite possible that crystal-packing constraints do not afford sufficient conformational flexibility in the mAChE gorge to provide strong transient electric fields and enable a reduction in transition state free energy and precise apposition of the azide and alkyne reactants for reactivity. That complexes of exquisite affinities can be formed with the synthetically generated *syn*- and *anti*-triazole compounds suggests an unusual synergism between occupation at the active center at the base of the gorge and the PAS at the rim, possibly driven by the coordinated side chain motions observed along the gorge path.

AUTHOR INFORMATION

Corresponding Authors

*yves.bourne@afmb.univ-mrs.fr

*pascale.marchot@univ-amu.fr

Notes

The authors declare no competing financial interest.

ACKNOWLEDGMENTS

We are grateful to M. Juin and S. Conrod (CNRS/AMU) for assistance in crystallization; G. Sulzenbacher, F. Vincent, S. Spinelli, M.C. Pelissier, M. Pesenti and I.P. Fabrichny (AFMB, CNRS/AMU) for X-ray data collection; R. Manetsch and A. Krasiński (Skaggs Institute of Chemical Biology, The Scripps Research Institute, La Jolla, CA) for the kind gift of the precursor and product inhibitors; and Z. Radić (SSPPS, UCSD) for fruitful discussions. Expert assistance from the MX beamline staff at the European Synchrotron Radiation Facility (Grenoble, France) is much appreciated. This work was supported by grants RO-1-GM18360-41 and UO1-NS 058046 (to PT), by CNRS grants "Action CNRS/USA" and "PICS" (to PM and YB), and by the French Infrastructure for Integrated Structural Biology (FRISBI) ANR-10-INSB-05-01.

REFERENCES

(1) Silman, I.; Sussman, J. L. *Curr. Opin. Pharmacol.* **2005**, *5*, 293.

(2) Taylor, P. In *Goodman and Gilman's The Pharmacological Basis of Therapeutics*; McGraw-Hill: New York, 2011.

(3) Sussman, J. L.; Harel, M.; Frolow, F.; Oefner, C.; Goldman, A.; Toker, L.; Silman, I. *Science* **1991**, *253*, 872.

(4) Silman, I.; Sussman, J. L. *Chem.-Biol. Interact.* **2008**, *175*, 3.

(5) Ripoll, D. R.; Faerman, C. H.; Axelsen, P. H.; Silman, I.; Sussman, J. L. *Proc. Natl. Acad. Sci. U. S. A.* **1993**, *90*, 5128.

(6) Tan, R. C.; Truong, T. N.; McCammon, J. A.; Sussman, J. L. *Biochemistry* **1993**, *32*, 401.

(7) Taylor, P.; Lappi, S. *Biochemistry* **1975**, *14*, 1989.

(8) Johnson, G.; Moore, S. W. *Curr. Pharm. Des.* **2006**, *12*, 217.

(9) Haviv, H.; Wong, D. M.; Silman, I.; Sussman, J. L. *Curr. Top. Med. Chem.* **2007**, *7*, 375.

(10) Kolb, H. C.; Sharpless, K. B. *Drug Discovery Today* **2003**, *8*, 1128.

(11) Mocharla, V. P.; Colasson, B.; Lee, L. V.; Röper, S.; Sharpless, K. B.; Wong, C. H.; Kolb, H. C. *Angew. Chem., Int. Ed.* **2004**, *44*, 116.

(12) Tron, G. C.; Pirali, T.; Billington, R. A.; Canonico, P. L.; Sorba, G.; Genazzani, A. A. *Med. Res. Rev.* **2008**, *28*, 278.

(13) Moorhouse, A. D.; Moses, J. E. *ChemMedChem* **2008**, *3*, 715.

(14) Mamidyala, S. K.; Finn, M. G. *Chem. Soc. Rev.* **2010**, *39*, 1252.

(15) Lewis, W. G.; Green, L. G.; Grynszpan, F.; Radić, Z.; Carlier, P. R.; Taylor, P.; Finn, M. G.; Sharpless, K. B. *Angew. Chem., Int. Ed.* **2002**, *41*, 1053.

(16) Manetsch, R.; Krasiński, A.; Radić, Z.; Raushel, J.; Taylor, P.; Sharpless, K. B.; Kolb, H. C. *J. Am. Chem. Soc.* **2004**, *126*, 12809.

(17) Krasiński, A.; Radić, Z.; Manetsch, R.; Raushel, J.; Taylor, P.; Sharpless, K. B.; Kolb, H. C. *J. Am. Chem. Soc.* **2005**, *127*, 6686.

(18) Bourne, Y.; Kolb, H. C.; Radić, Z.; Sharpless, K. B.; Taylor, P.; Marchot, P. *Proc. Natl. Acad. Sci. U. S. A.* **2004**, *101*, 1449.

(19) Bourne, Y.; Radić, Z.; Taylor, P.; Marchot, P. *J. Am. Chem. Soc.* **2010**, *132*, 18292.

(20) Radic, Z.; Pickering, N. A.; Vellom, D. C.; Camp, S.; Taylor, P. *Biochemistry* **1993**, *32*, 12074.

(21) Bourne, Y.; Radic, Z.; Sulzenbacher, G.; Kim, E.; Taylor, P.; Marchot, P. *J. Biol. Chem.* **2006**, *281*, 29256.

(22) Bourne, Y.; Radić, Z.; Aráoz, R.; Talley, T. T.; Benoit, E.; Servent, D.; Taylor, P.; Molgó, J.; Marchot, P. *Proc. Natl. Acad. Sci. U. S. A.* **2010**, *107*, 6076.

(23) Kabsch, W. *Acta Crystallogr., Sect. D: Biol. Crystallogr.* **2010**, *66*, 133.

(24) CCP4. *Acta Crystallogr., Sect. D: Biol. Crystallogr.* **1994**, *50*, 760.

(25) Bourne, Y.; Taylor, P.; Radić, Z.; Marchot, P. *EMBO J.* **2003**, *22*, 1.

(26) Murshudov, G. N.; Vagin, A. A.; Dodson, E. J. *Acta Crystallogr., Sect. D: Biol. Crystallogr.* **1997**, *53*, 240.

(27) Bricogne, G.; Blanc, E.; Brandl, M.; Flensburg, C.; Keller, P.; Paciorek, W.; Roversi, P.; Sharff, A.; Smart, O. S.; Vonrhein, C.; Womack, T. O. *BUSTER*, version 2.11.2; Global Phasing Ltd.: Cambridge, United Kingdom, 2011.

(28) Emsley, P.; Cowtan, K. *Acta Crystallogr., Sect. D: Biol. Crystallogr.* **2004**, *60*, 2126.

(29) Davis, I. W.; Leaver-Fay, A.; Chen, V. B.; Block, J. N.; Kapral, G. J.; Wang, X.; Murray, L. W.; Arendall, W. B.; Snoeyink, J.; Richardson, J. S.; Richardson, D. C. *Nucleic Acids Res.* **2007**, *35*, W375.

(30) Liang, J.; Edelsbrunner, H.; Woodward, C. *Protein Sci.* **1998**, *7*, 1884.

(31) *The PyMOL Molecular Graphics System*, Version 1.5.0.4; Schrödinger, LLC, 2010.

(32) Senapati, S.; Cheng, Y.; McCammon, J. A. *J. Med. Chem.* **2006**, *49*, 6222.

(33) Morris, G. M.; Green, L. G.; Radić, Z.; Taylor, P.; Sharpless, K. B.; Olson, A. J.; Grynszpan, F. *J. Chem. Inf. Model.* **2013**, *53*, 898.

(34) Shen, T.; Tai, K.; Henchman, R. H.; McCammon, J. A. *Acc. Chem. Res.* **2002**, *35*, 332.

(35) Harel, M.; Schalk, I.; Ehret-Sabatier, L.; Bouet, F.; Goeldner, M.; Hirth, C.; Axelsen, P. H.; Silman, I.; Sussman, J. L. *Proc. Natl. Acad. Sci. U. S. A.* **1993**, *90*, 9031.

(36) Millard, C. B.; Koellner, G.; Ordentlich, A.; Shafferman, A.; Silman, I.; Sussman, J. L. *J. Am. Chem. Soc.* **1999**, *121*, 9883.

(37) (a) Artursson, E.; Andersson, P. O.; Akfur, C.; Linusson, A.; Börjegren, S.; Ekström, F. *Biochem. Pharmacol.* **2013**, *85*, 1389. (b) References 8 and 13 herein. (c) References 10 and 30 herein.

(38) Radisky, E. S.; Lee, J. M.; Lu, C. J.; Koshland, D. E. *Proc. Natl. Acad. Sci. U. S. A.* **2006**, *103*, 6835.

(39) Congreve, M. S.; Davis, D. J.; Devine, L.; Granata, C.; O'Reilly, M.; Wyatt, P. G.; Jhoti, H. *Angew. Chem., Int. Ed.* **2003**, *42*, 4479.

(40) Yamane, J.; Ohyabu, N.; Yao, M.; Takemoto, H.; Tanaka, I. *J. Appl. Crystallogr.* **2010**, *43*, 1329.

(41) Wischeler, J. S.; Sun, D.; Sandner, N. U.; Linne, U.; Heine, A.; Koert, U.; Klebe, G. *Chem. - Eur. J.* **2011**, *17*, 5842.

(42) Dirksen, A.; Hackeng, T. M.; Dawson, P. E. *Angew. Chem., Int. Ed.* **2006**, *45*, 7581.

DOI: 10.1021/jacs.5b11384
J. Am. Chem. Soc. 2016, 138, 1611−1621

(43) Bunyapaiboonsri, T.; Ramström, O.; Lohmann, S.; Lehn, J. M.; Peng, L.; Goeldner, M. *ChemBioChem* **2001**, *2*, 438.
(44) Radić, Z.; Manetsch, R.; Fournier, D.; Sharpless, K. B.; Taylor, P. *Chem.-Biol. Interact.* **2008**, *175*, 161.
(45) Oueis, E.; Santoni, G.; Ronco, C.; Syzgantseva, O.; Tognetti, V.; Joubert, L.; Romieu, A.; Weik, M.; Jean, L.; Sabot, C.; Nachon, F.; Renard, P. Y. *Org. Biomol. Chem.* **2014**, *12*, 156.
(46) Fried, S. D.; Bagchi, S.; Boxer, S. G. *Science* **2014**, *346*, 1510.
(47) Levinson, N. M.; Boxer, S. G. *Nat. Chem. Biol.* **2014**, *10*, 127.
(48) Grimster, N. P.; Stump, B.; Fotsing, J. R.; Weide, T.; Talley, T. T.; Yamauchi, J. G.; Nemecz, A.; Kim, C.; Ho, K. Y.; Sharpless, K. B.; Taylor, P.; Fokin, V. V. *J. Am. Chem. Soc.* **2012**, *134*, 6732.
(49) Radic, Z.; Taylor, P. *J. Biol. Chem.* **2001**, *276*, 4622.
(50) Abboud, J.-L. M.; Foces-Foces, C.; Notario, R.; Trifonov, R. E.; Volovodenko, A. P.; Ostrovskii, V. A.; Alkorta, I.; Elguero, J. *Eur. J. Org. Chem.* **2001**, *2001*, 3013.

DOI: 10.1021/jacs.5b11384
J. Am. Chem. Soc. 2016, 138, 1611−1621